Three-center tight-binding potential model for C and Si

Wen-Cai Lu, C. Z. Wang, Li-Zhen Zhao, Wei Qin, and K. M. Ho

Phys. Rev. B **92**, 035206 — Published 29 July 2015

DOI: 10.1103/PhysRevB.92.035206

A 3-center tight-binding potential model for C and Si

Wen-Cai Lu,[a,§] C. Z. Wang,[b,*] Li-Zhen Zhao,[a] Wei Qin,[a] K. M. Ho[b]

[a]*College of Physics and Laboratory of Fiber Materials and Modern Textile, the Growing Base for State Key Laboratory, Qingdao University, Qingdao, Shandong 266071, P.R. China*

[b]*Ames Laboratory-U.S. DOE and Department of Physics and Astronomy, Iowa State University, Ames, IA 50011, U.S.A.*

Abstract

A tight-binding potential model which goes beyond the Slater-Koster two-center approximation and includes explicit 3-center and crystal field expressions is presented. Using carbon and silicon as examples, we show that various bulk structures, surface reconstructions, and the structures of clusters and liquids of C and Si can be well described by the present 3-center tight-binding model. These results demonstrate that 3-center interaction and crystal field effect are very important for improving the transferability of tight-binding models in describing the structures and properties of materials over a broad range of bonding configurations.

PACS Numbers: 31.15.bu, 71.15.-m, 61.50.Lt, 61.20.Ja

[*] wangcz@ameslab.gov

[§] wencailu@jlu.edu.cn

I. INTRODUCTION

The tight-binding (TB) method is an important empirical method, which has attracted continuous interests for many years since it was proposed by Slater and Koster in 1954 [1-16]. The main advantage of the TB method is its fast computational speed due to the use of minimal basis set and parameterized Hamiltonian and overlap matrices. However, the transferability of the TB parameterization has been the key bottleneck hindering wide-spread applications of the TB method. As an extension of the empirical TB method towards density functional theory (DFT), the density functional based TB (DFTB) method [17-22] is in popular use today. The DFTB method was proposed in 1995 [17], shortly afterwards it was modified from non-self-consistent redistribution of charges (non-SCC) [17,18] to SCC version [19] in which a second-order expansion of the DFT total energy functional with respect to charge density fluctuations is employed. In the DFTB method, a parameter-free expression of two-center Hamiltonian matrix within a basis (usually a minimal basis) of confined atomic orbitals can be explicitly derived [17]. However, a parameterization for repulsive terms is still required.

The DFTB and most of the commonly used TB potential models so far are based on the two-center approximation of Hamiltonian proposed by Slater and Koster [1], which assumes that the potential part of the Hamiltonian is a sum of spherical potentials centered on the pair of atoms. Using a transformation that brings the wave functions from first-principles calculations onto a set of quasiatomic minimal basis orbitals (QUAMBOs), Lu *et al.* [15] and Chan *et al.* [16] were able to extract accurate Hamiltonian and overlap matrix elements directly from first-principles wave functions. These Hamiltonian matrix elements down-folded from the DFT calculations can include the multi-center interaction and large basis effects. It was found that although the TB overlap matrix elements can be well described by the Slater-Koster two-center integrals, the two-center approximation is not adequate for the Hamiltonian matrix elements [15,16].

Many studies over the past twenty years have also indicated that the transferability of the TB models based on the two-center approximation of

Hamiltonian is limited, particularly for structures with metallic behavior [9-14]. Several empirical approaches to include 3-center interactions, e.g. by rescaling the hopping between a pair of atoms according to bonding environments of the pair, have been proposed [9-14]. Although such environment-dependent TB models have shown some improvements over the previous two-center TB models, *ad hoc* empirical functions have to be introduced to mimic the 3-center interaction and crystal field effect.

In this paper, we proposed a 3-center TB (3c-TB) potential model which goes beyond the two-center TB model and includes explicitly 3-center interaction and crystal field effect. Applications of the model to carbon and silicon indicate that the model exhibits good accuracy and transferability in describing various carbon and silicon structures including bulk phases, surfaces, clusters, and high temperature liquids.

II. 3c-TB POTENTIAL MODEL

The binding energy of a system in our 3c-TB potential model is represented by

$$E_{bind} = \sum_{n\in occ} \varepsilon_n - \sum_{i,\alpha\in occ} \varepsilon^0_{i\alpha} + E_{rep} \tag{1}$$

where $\varepsilon^0_{i\alpha}$ are the energy levels for atomic valence orbital α of atom i. As a stationary approximation, also known as the "Harris-Foulkes" approximation [23,24], to the self-consistent density functional theory (DFT) with frozen-core potentials, ε_n are the eigenvalues of a non-self-consistent one-electron equation of the form [25]

$$\left\{-\frac{1}{2}\nabla^2 + V_{nucl}(\mathbf{r}) + V_H[n_v(\mathbf{r})] + \mu_{xc}[n_v(\mathbf{r})]\right\}\psi_n = \varepsilon_n\psi_n \tag{2}$$

In Eq. (2), $n_v(\mathbf{r})$ is the valence density, V_{nucl} the ion potential, V_H the Hartree potential,

$$V_H = \int \frac{n_v(\mathbf{r}')}{|\mathbf{r}-\mathbf{r}'|} d\mathbf{r}' \tag{3}$$

and μ_{xc} the exchange-correlation potential,

$$\mu_{xc} = \frac{\partial E_{xc}}{\partial n_v(\mathbf{r})} \tag{4}$$

Then, E_{rep} in Eq. (1) is expressed by

$$E_{rep} = \frac{1}{2}\sum_{i\neq j}\frac{Z_{vi}Z_{vj}}{\mathbf{R}_i - \mathbf{R}_j} - \frac{1}{2}\int V_H[n_v]\, n_v d\mathbf{r} - \int \mu_{xc}[n_v]\, n_v d\mathbf{r} + E_{xc}[n_v] + \sum_i \frac{1}{2}\int V_H[n_{vi}^0]\, n_{vi}^0 d\mathbf{r} + \sum_i \int \mu_{xc}[n_{vi}^0]\, n_{vi}^0 d\mathbf{r} - \sum_i E_{xc}[n_{vi}^0] \quad (5)$$

In Eq. (5), Z_{vi}, Z_{vj} are the numbers of valence electrons on the atoms i and j at $\mathbf{R}_i$ and $\mathbf{R}_j$, n_{vi}^0 the valence density of isolated free atom, and E_{xc} the exchange-correlation functional. Thus, E_{rep} is a repulsive energy function which includes the ion-ion repulsive energies and the subtraction of the over-counting of the Hartree interactions and a correction of the electron exchange-correlation in both $\sum_{n\in occ}\varepsilon_n$ and $\sum_{i,\alpha\in occ}\varepsilon_{i\alpha}^0$ in Eq. (1).

For a set of the sp^3 minimal basis orbitals, the Hamiltonian matrix elements in the Slater and Koster two-center formulae [1] can be expressed by

$$\begin{aligned}
H_{is,js}^{2c} &= h_{ss} \\
H_{is,jpx}^{2c} &= c_x h_{sp} \\
H_{is,jpy}^{2c} &= c_y h_{sp} \\
H_{is,jpz}^{2c} &= c_z h_{sp} \\
H_{ipx,jpx}^{2c} &= c_x^2 h_{pp\sigma} - (1-c_x^2) h_{pp\pi} \\
H_{ipy,jpy}^{2c} &= c_y^2 h_{pp\sigma} - (1-c_y^2) h_{pp\pi} \\
H_{ipz,jpz}^{2c} &= c_z^2 h_{pp\sigma} - (1-c_z^2) h_{pp\pi} \\
H_{ipx,jpy}^{2c} &= c_x c_y (h_{ppo} - h_{pp\pi}) \\
H_{ipy,jpz}^{2c} &= c_y c_z (h_{ppo} - h_{pp\pi}) \\
H_{ipx,jpz}^{2c} &= c_x c_z (h_{ppo} - h_{pp\pi})
\end{aligned} \quad (6)$$

in which c_x, c_y, and c_z are directional cosines defined by $c_x = (x_j - x_i)/r_{ij}$, $c_y = (y_j - y_i)/r_{ij}$, and $c_x = (z_j - z_i)/r_{ij}$, and h_{ss}, h_{sp}, $h_{pp\sigma}$, and $h_{pp\pi}$, are called hopping integrals.

In our 3c-TB potential model, the important 3-center interaction is explicitly included into the TB Hamiltonian matrix to calculate the band-structure energy. The 3-center potential part of the Hamiltonian, H^{3c}, involving the potential ($-V_A$) on the third-party atom A, can be expressed as

$$H_{i\alpha,j\beta}^{3c} = -\sum_A \int \phi_{i\alpha}^*(\mathbf{r}-\mathbf{R}_i)\; V_A(\mathbf{r}-\mathbf{R}_A)\phi_{j\beta}(\mathbf{r}-\mathbf{R}_j)d\mathbf{r} \quad (7)$$

where i and j are the pair of atoms and $\phi_{i\alpha}$ and $\phi_{i\beta}$ represent quasiatomic orbitals.

We can expand $\phi_{i\alpha}$ and $\phi_{i\beta}$ on (i, j) into a set of the quasiatomic orbitals $\phi_{A\lambda}$ on A:

$$\phi_{i\alpha}(\mathbf{r}-\mathbf{r}_i) \approx \sum_{\lambda} \left\langle \phi_{A\lambda}(\mathbf{r}-\mathbf{R}_A) \middle| \phi_{i\alpha}(\mathbf{r}-\mathbf{R}_i) \right\rangle \ \phi_{A\lambda}(\mathbf{r}-\mathbf{R}_A) = \sum_{\lambda} S_{A\lambda,i\alpha}\phi_{A\lambda}(\mathbf{r}-\mathbf{R}_A) \tag{8}$$

In Eq. (8), S is the overlap matrix in the space of non-orthogonal minimal basis orbitals. Under the spherical approximation for $-V_A$, we have

$$\begin{aligned} \left\langle \phi_{A\lambda}(\mathbf{r}-\mathbf{R}_\mathbf{A}) \middle| -V_A(\mathbf{r}-\mathbf{R}_\mathbf{A}) \middle| \phi_{A\lambda'}(\mathbf{r}-\mathbf{R}_\mathbf{A}) \right\rangle &\approx -\left\langle \phi_{A\lambda}(\mathbf{r}) \middle| V_A(r) \middle| \phi_{A\lambda}(\mathbf{r}) \right\rangle \\ &= -\left\langle \phi^R_{A,nl}(r) \middle| V_A(r) \middle| \phi^R_{A,n'l}(r) \right\rangle \end{aligned} \tag{9}$$

where indices $\{n, l\}$ represent principle and angular quantum numbers and ϕ^R is the radial part of orbital ϕ. If we only hold the large diagonal terms with $n = n'$ and thus $\lambda = \lambda'$, then

$$\begin{aligned} H^{3c}_{i\alpha,j\beta} &= \sum_{A\lambda\lambda'} S^*_{A\lambda,i\alpha} S_{A\lambda',j\beta} \left\langle \phi_{A\lambda}(\mathbf{r}-\mathbf{R}_A) \middle| -V_A(\mathbf{r}-\mathbf{R}_A) \middle| \phi_{A\lambda'}(\mathbf{r}-\mathbf{R}_A) \right\rangle \\ &\approx -\sum_{A\lambda} S^*_{A\lambda,i\alpha} S_{A\lambda,j\beta} \left\langle \phi_{A\lambda}(\mathbf{r}) \middle| V_A(r) \middle| \phi_{A\lambda}(\mathbf{r}) \right\rangle \\ &= -\sum_{A\lambda} B_{i\alpha,A\lambda} B_{A\lambda,j\beta} \end{aligned} \tag{10}$$

with

$$\begin{aligned} B_{i\alpha,A\lambda} &= S_{i\alpha,A\lambda} \ \left\langle \phi_{A\lambda}(\mathbf{r}) \middle| \, | V_A(r) | \, \middle| \phi_{A\lambda}(\mathbf{r}) \right\rangle^{1/2} \\ B_{A\lambda,j\beta} &= S_{A\lambda,j\beta} \ \left\langle \phi_{A\lambda}(\mathbf{r}) \middle| \, | V_A(r) | \, \middle| \phi_{A\lambda}(\mathbf{r}) \right\rangle^{1/2} \end{aligned} \tag{11}$$

Thus, the 3-center interaction can be approximated by a sum of products of two hoppings (*Bs*).

Similarly, the crystal field effect on the on-site Hamiltonian matrix elements can also be evaluated using the same formula as Eq. (10) with $i = j$:

$$H^{cf}_{i\alpha,i\beta} = -\sum_{A\lambda} C_{i\alpha,A\lambda} C_{A\lambda,i\beta} \tag{12}$$

By including the corrections of H^{3c} and H^{cf}, the TB Hamiltonian matrix elements become

$$H_{ij\,(i\neq j)} = \left\{ \ (H^{2c}_{i\alpha,j\beta} + H^{3c}_{i\alpha,j\beta}) \ \right\} \tag{13}$$

$$H_{ii} = \left\{ \ (\varepsilon^0_{i\alpha}\delta_{\alpha\beta} + H^{cf}_{i\alpha,i\beta}) \ \right\} \tag{14}$$

For the sp^3 quasiatomic minimal basis, Eqs. (13) and (14) can be expressed in the

following matrix forms

$$H_{ij(i\neq j)} = \left\{ \overbrace{\begin{matrix} H_{is,js} & H_{is,jpx} & H_{is,jpy} & H_{is,jpz} \\ H_{ipx,js} & H_{ipx,jpx} & H_{ipx,jpy} & H_{ipx,jpz} \\ H_{ipy,js} & H_{ipy,jpx} & H_{ipy,jpy} & H_{ipy,jpz} \\ H_{ipz,js} & H_{ipz,jpx} & H_{ipz,jpy} & H_{ipz,jpz} \end{matrix}}^{H^{2c}_{i\alpha,j\beta}+H^{3c}_{i\alpha,j\beta}} \right\} \tag{15}$$

and

$$H_{ii} = \left\{ \begin{matrix} \varepsilon^0_{is} + H^{cf}_{is,is} & H^{cf}_{is,ipx} & H^{cf}_{is,ipy} & H^{cf}_{is,ipz} \\ H^{cf}_{ipx,is} & \varepsilon^0_{ip} + H^{cf}_{ipx,ipx} & H^{cf}_{ipx,ipy} & H^{cf}_{ipx,ipz} \\ H^{cf}_{ipy,is} & H^{cf}_{ipy,ipx} & \varepsilon^0_{ip} + H^{cf}_{ipy,ipy} & H^{cf}_{ipy,ipz} \\ H^{cf}_{ipz,is} & H^{cf}_{ipz,ipx} & H^{cf}_{ipz,ipy} & \varepsilon^0_{ip} + H^{cf}_{ipz,ipz} \end{matrix} \right\} \tag{16}$$

Therefore, the 3-center and crystal field terms are explicitly included in the Hamiltonian matrix.

The distance dependence of the two-center integral is modeled by

$$h_\mu (\text{or } s_\mu) = a_1 r^{a_2} [(1 - e^{-a_3 (r - a_4)})^2 - 1] \tag{17}$$

where r is the distance between two atoms, and a_1 to a_4 are 4 parameters obtained by fitting to the first-principles calculated data. In this work, the angular dependence of Slater-Koster approach (Eq. (6)) is adapted for all two-center integrals including the B and C terms in the 3-center interaction and crystal field, thus the symmetry properties inherited from the basis orbitals are correctly incorporated. However, the angular dependence of the TB potential in our 3-center model is different from that in the Slater-Koster theory due to the $B \times B$ and $C \times C$ terms.

Figure 1 illustrates the main difference between the present 3c-TB potential model and traditional Slater-Koster two-center TB model. According to the Slater-Koster theory, when the standard sp^3 atomic orbitals are used as a basis for the local geometry as shown in Fig. 1 (e.g. a Si_3 cluster), the hopping matrix elements $H^{2c}_{1s,2pz}$, $H^{2c}_{1py,2pz}$ and their conjugated terms between atoms 1 and 2 should be zero. In

addition, the on-site TB matrix elements should be all zero except for the diagonal ones which are equal to the *s* and *p* atomic orbital energies. However, for the Si_3 cluster with the geometry shown in Fig. 1, the Hamiltonian matrix elements down-folded from the DFT-PBE calculations and based on the QUAMBOs (Table I) show that these matrix elements are far from being zero. Moreover the crystal field also leads to a splitting of three *p*-orbital energy levels which are degenerate in the Slater-Koster theory. Note that the Hamiltonian matrix down-folded from the DFT-PBE calculations using the QUAMBO analysis contains the 3-center interaction, crystal field effect, and also large basis effect, and it reproduces exactly the occupied molecular orbital energy levels or the valence bands. It is obvious from Table I that the 3c-TB Hamiltonian matrix $H^{3c\text{-}TB}$ of Si_3 captures the non-zero matrix elements that were missed in the Slater-Koster two-center approximation. These results suggest that the angular dependence of the Hamiltonian matrix elements is more general and robust in the present 3c-TB potential model than in the Slater-Koster two-center approach.

Although the QUAMBOs down-folded from a large basis deform with their bonding environment, the overlap matrix of QUAMBOs [15] can be pretty well described by the Slater-Koster two-center form

$$S_{i\alpha,j\beta} = S^{2c}_{i\alpha,j\beta} \tag{18}$$

Thus the 3c-TB overlap matrix is still evaluated by a two-center formalism.

In previous studies, the repulsive energy function E_{rep} was usually approximated by pairwise potentials or pairwise potentials multiplied by environment-dependent screening factors [12,13,17,19,26,27]. In this paper, we introduce an explicit 3-center term into E_{rep}

$$E_{rep} = \frac{1}{2}\sum_{i,j}(\chi_{ij} - \sum_{A}\chi^{3c}_{iA}\chi^{3c}_{Aj}) \tag{19}$$

with

$$\chi\,(or\ \chi^{3c}) = a_1 r^{a_2}\ \mathrm{e}^{-a_3 r^{a_4}} \tag{20}$$

where χ is a pairwise repulsive potential, and χ^{3c} represents the environment-

dependent effect caused by the third-party atom A.

In addition we have 3 parameters r_{max}, r_{mathc} and r_{min} to describe the interaction range (see Table II), in which r_{max} is the cutoff distance of the interaction, r_{match} is the starting point at which an attenuation function is multiplied, i.e., for $r_{match} < r < r_{max}$ the hoppings (h, h^B and h^C), overlap (s), and repulsive functions (χ and χ^{3c}) are in the form

$$\mu = \mu \times \cos^2\left(\frac{\pi}{2}\frac{r - r_{match}}{r_{max} - r_{match}}\right) \quad (r_{match} < r < r_{max}) \tag{21}$$

where μ indicates h, h^B, h^C, s, χ and χ^{3c}. The interaction range is large enough so that the 3c-TB potential for carbon can also describe the interaction between the graphite layers. Besides, one parameter r_{min} is set to avoid the possible abnormal behavior of hopping or overlap expressions at small interaction distances. For $r < r_{min}$ we hold $\mu(r) = \mu(r_{min})$ ($\mu = h$, h^B, h^C and s), while the repulsive terms χ and χ^{3c} are not submitted to this setup, i.e.,

$$\mu(r) = \mu(r_{\min}) \quad (r < r_{\min} \text{ and } \mu = h, h^B, h^C \text{ and } s) \tag{22}$$

The approximations in the 3-center interaction and crystal field effect in the 3c-TB potential model are from the spherical assumption of the potential $-V_A$ on the third part atom and the expansion of the minimal basis orbitals of the interacting pair of atoms (i, j) by the minimal basis orbitals $\phi_{A\lambda}$ at the third-party atom site. Enough basis orbitals on the site A in Eq. (8) would be required for accurate expansion of atomic orbitals $\phi_{i\alpha}$ and $\phi_{i\beta}$. In this paper, only minimal basis orbitals with s, px, py and pz characters are used to develop the 3c-TB potential model for C and Si. The errors due to the approximation discussed above will be compensated through the parameter fitting.

The 3c-TB potential model described above is applied to determine the 3c-TB parameters for carbon and silicon by fitting to a first-principles DFT database including the binding energies, band structures or molecular orbital energy levels, and Hamiltonian and overlap matrix elements of various structures. For each potential model, 22, 10, and 8 parameters are used to describe the 3c-TB Hamiltonian matrix,

the overlap matrix, and the repulsive energy terms, respectively. There are also 2 parameters for *s* and *p* orbital energies (ε_s and ε_p), and 3 parameters (r_{max}, r_{match} and r_{min}) describing the interaction range as denoted in Table II

III. 3c-TB CALCULATED RESULTS FOR C AND Si COMPARED WITH THE DFT RESULTS

A. Bands for several crystalline phases

Figures 2 and 3 show the calculated band structures for C in the diamond, graphene, simple cubic (SC), and body-centered cubic (BCC) structures, and Si in the diamond, SC, BCC and face-centered cubic (FCC) structures, by using the 3c-TB, the DFTB$^+$ [19,22], and the DFT-PW91 implemented in VASP [28,29]. In the DFT calculations, plan-wave basis sets corresponding to the kinetic energy cutoffs of 400 eV (C) and 245 eV (Si) were adopted. The calculations of binding energies and charge consistency before the band structure calculations were performed using the Monkhorst-Pack mesh k-points grid of $12 \times 12 \times 12$ for diamond, BCC and FCC, $12 \times 12 \times 1$ for graphene, $16 \times 16 \times 16$ for SC , and $10 \times 10 \times 20$ for the β-tin structure.

The 3c-TB potential model describes well the valence bands of C and Si. The Dirac point in the graphene bands is also well reproduced by the 3c-TB calculation. Due to the adoption of the minimal basis set in the 3c-TB and DFTB methods, the conduction bands from the first-principles calculations cannot be reproduced accurately by the 3c-TB and DFTB calculations. The band gaps of C and Si in the diamond structures are 4.56 (C) and 1.47 eV (Si) by 3c-TB, compared with the band gaps of 6.90 eV (C) and 1.27 eV (Si) by DFTB and 4.15 eV (C) and 0.64 eV (Si) by DFT-PW91. It is also interesting to note that although the band gap for silicon in the diamond structure is larger than that from the DFT-PW91 calculation, the indirect band gap feature, which is very difficult to be reproduced by semi-empirical and minimal basis calculations, is well described by the 3c-TB potential model.

B. Binding energies of crystalline phases and surfaces

The comparison of the binding energy curves from the 3c-TB, DFTB and DFT

calculations for C and Si in various crystalline structures is shown in Fig. 4. In general, the 3c-TB and the DFTB methods reproduce well the first-principles DFT calculation results, suggesting that they exhibit a good transferability over a wide range of bonding environments. For the metallic phases (e.g. SC. BCC, FCC), the 3c-TB gives a better description of the binding energy curves than the DFTB does (Fig. 4), indicating that the effects of 3-center interactions and crystal field are important for systems with metallic behavior.

We have also tested the accuracy and transferability of the 3c-TB potential model by applying it to studying various reconstructions on C (100) and C (111) as well as Si (100) and Si (111) surfaces. The surface energies of the C (100) 2 × 1 symmetric dimer raw and C (111) 2 × 1 Pandey π-bonded chain reconstructed surfaces from the 3c-TB calculations are 1.96 and 1.39 eV per surface atom, respectively, which are in good agreement with the first-principles calculated results of 2.12 and 1.346 eV [30]. For the Si (100) surface, the surface energies of the (1 × 1), asymmetric (2 × 1) and *c* (4 × 2) surface structures obtained from our calculations are 1.98, 1.21 and 1.15 eV per surface atom, respectively, in good agreement with the DFT calculated results of 2.174, 1.321 and 1.285 eV [31]. For the Si (111) surface, the 3c-TB potential model predicts that the surface energies of the (1× 1), (2 × 1) π-bonded chain, and (7 × 7) dimer–adatom–stacking-fault (DAS) are 1.343, 1.089, and 1.061 eV per surface atom, respectively, which compare well with the first-principles calculated results of 1.435, 1.141 and 1.073 eV [31], showing that the (7 × 7) is the most stable structure among the Si (111) surface reconstructions from the present 3c-TB calculations.

C. Binding energies of clusters

Another challenging test for the accuracy and transferability of TB potentials is the studies of clusters. Accurate predictions of energy orders of various cluster isomers are very challenging because bonding characters on cluster surface are complex and many cluster isomers are close in energy. Using the 3c-TB potentials developed above, we have studied the energy orders of a series of carbon cluster isomers in the range of 6 to 34 atoms [32-35] and silicon cluster isomers in the size

range of 7 to 78 atoms [36,37]. For carbon clusters, isomers with linear, ring, cage, plate and bowl motifs [32-35] have been considered. These clusters were fully relaxed using the 3c-TB method.

As we can see from Fig. 5, the energy orders of various C and Si cluster isomers predicted from the 3c-TB and DFTB methods in general agree well with those from the DFT calculations performed using the GAUSSIAN03 package [38]. The good agreements between the 3c-TB and DFT binding energies per atom (E_b) or between the DFTB and DFT E_bs can also be seen from Fig. 6, in which the scatter plots of $E_b^{3c\text{-}TB}$ versus E_b^{DFT} or E_b^{DFTB} versus E_b^{DFT} can be accurately fitted by a linear function with very small standard errors. For carbon clusters, the standard errors are 9.5×10^{-4} and 12.6×10^{-4} eV for the 3c-TB and DFTB, respectively. For silicon clusters, these errors are 3.8×10^{-4} (3c-TB) and 6.3×10^{-4} eV (DFTB). The geometries of the clusters after the TB relaxations are also very similar to those from the first-principles DFT calculations as one can see from the examples shown in Fig. 7. One exception for the lowest energy structure in the small cluster range is C_6. The 3c-TB and DFTB calculations predict that the linear structure of C_6 is lower in energy than the D_{3h} ring structure, while most of *ab initio* calculations show that the D_{3h} ring structure is slightly more stable than the linear one and the two isomers are close in energy [32]. In the experiment, the linear structure of C_6 has been observed [39,40].

D. MD simulations - Liquids

We have also performed molecular dynamics (MD) simulations to study the structures of carbon and silicon in the liquid state. The simulations were performed with a cubic unit cell containing 512 atoms and with periodic boundary conditions. The atoms were initially arranged in random positions within the cubic unit cell. In this work, the test for liquid carbon has been performed at a density of 2.9 g/cm^3 and a temperature of 5000 K in order to compare with the available first-principles MD simulations result [41]. Hot carbon liquid was first prepared at 7000 K and then cooled down to 5000 K to measure the structural properties. For liquid silicon, the MD simulation was performed at a density of 2.53 g/cm^3 and a temperature of 1793 K

where the results from the first-principles MD simulation [42] are also available for comparison. For liquid silicon, the system was firstly heated to 2500 K to have the liquid phase well prepared and then cooled down to 1793 K and well thermally equilibrated at this temperature. The MD trajectories were collected for more than 5000 MD steps for statistical mechanical analyses of structure and thermodynamics properties of the liquids.

As we can see from Fig. 8, the results from the 3c-TB simulations agree well with those from the first-principles MD simulations. The coordination numbers of the liquids, obtained by integration of the *g(r)* up to their first minimum (1.92 Å for carbon and 3.12 Å for silicon), are 3.34 for liquid carbon and 6.39 for liquid silicon. The coordination number of 6.39 for liquid Si agrees well the values estimated from the first-principles MD simulations [42,43], indicating that liquid silicon at this temperature is metallic [43]. The coordination number of 3.34 for liquid carbon indicates that the liquid carbon at the density of 2.9 g/cm^3 and temperature of 5000 K consists of mixed sp^2 and sp^3 bonds. The ratio of sp^2 to sp^3 bonds is about 2. Considering that the liquid structures are not used in the fitting database to determine the parameters, such good agreements suggest that the 3c-TB model has good accuracy as well as transferability.

IV. CONCLUSIONS

We have presented a new 3c-TB potential model with applications to C and Si systems. The 3-center interaction and crystal field effect are incorporated through a production of two two-center integral expressions. The accuracy and transferability of the 3c-TB over bulk structures, surfaces, and especially clusters and liquids were shown by the well agreements with the first-principles DFT results. One of the important differences between the 3c-TB and the DFTB is that the 3-center integral expression and crystal field effect are included explicitly in the 3c-TB potential model while the DFTB is based on the two-center Hamiltonian matrix elements. Moreover, because our 3c-TB parameters are derived by a data fitting to the first-principles calculated results under a large basis set (including the binding energies, band

structures or orbital energy levels, and Hamiltonian and overlap matrix elements), the effect of large basis set is included. As discussed in the text, the 3-center integrals and crystal field are important for accurate description of metallic phases (e.g., SC, BCC, FCC phases of C and Si and liquid phase of Si in this paper). We believe that the 3c-TB potential model described in this paper will be useful for modeling and simulation of such systems. While the 3c-TB method was applied to C and Si with the sp^3 quasiatomic orbitals, an extension of the model to the transition metal elements with extra *d* valence orbitals is straightforward. The good transferability and accuracy of the 3c-TB potential model is anticipated to widen its applications in large-scale atomistic calculations of nanostructures and materials.

ACKNOWLEDGMENTS

Ames Laboratory is operated for the U.S. Department of Energy by Iowa State University under Contract No. DE-AC02-07CH11358. Work at Ames Laboratory was supported by the Director for Energy Research, Office of Basic Energy Sciences, Division of Material Science and Engineering including a grant for computer time at the National Energy Research Scientific Computing Center (NERSC) in Berkeley, CA. This work is also supported by the National Natural Science Foundation of China (Grant No. 21273122). Lizhen Zhao acknowledges the support by the National Natural Science Foundation of China (Grant No. 21203105) and Wei Qin acknowledges the support by the China Postdoctoral Science Foundation (Grant No. 2014M561885).

References

[1] J. C. Slater and G. F. Koster, Phys. Rev. **94**, 1498 (1954).

[2] D. J. Chadi, Phys. Rev. Lett. **43**, 43 (1979).

[3] W. A. Harrison, Electronic Structure and the Properties of Solids (Freeman, San Francisco 1980).

[4] C. Z. Wang, C. T. Chan, and K. M. Ho, Phys. Rev. B **39**, 8592 (1989).

[5] L. Goodwin, A. J. Skinner, and D. G. Pettifor, Europhys. Lett. **9**, 701 (1989).

[6] C. H. Xu, C. Z. Wang, C. T. Chan, and K. M. Ho, J. Phys.: Condens. Matt. **4**, 6047 (1992).

[7] L. Colombo, Ann. Rev. Comp. Phys. **147** (IV), 1 (1996).

[8] D. Porezag, Th. Frauenheim, Th. Köhler, G. Seifert, and R. Kaschner, Phys. Rev. B **51**, 12947 (1995).

[9] J. L. Mercer, Jr. and M. Y. Chou, Phys. Rev. B **47**, 9366 (1993); Phys. Rev. B **49**, 8506 (1994).

[10] M. J. Mehl and D. A. Papaconstantopoulos, J. Phys.: Condens. Matt. **15**, R413 (2003).

[11] N. Bernstein, M. J. Mehl, and D. A. Papaconstantopoulos, Phys. Rev. B **66**, 075212 (2002).

[12] M. S. Tang, C. Z. Wang, C. T. Chan, and K. M. Ho, Phys. Rev. B **53**, 979 (1996).

[13] C. Z. Wang, B. C. Pan, and K. M. Ho, J. Phys.: Condens. Matt. **11**, 2043 (1999).

[14] M. Yu, S. Y. Wu, and C. S. Jayanthi, Physica E **42**, 1 (2009).

[15] W. C. Lu, C. Z. Wang, K. Ruedenberg, and K. M. Ho, Phys. Rev. B **72**, 205123 (2005).

[16] T. L. Chan, Y. X. Yao, C. Z. Wang, W. C. Lu, J. Li, X. F. Qian, S. Yip, and K. M. Ho, Phys. Rev. B **76**, 205119 (2007).

[17] D. Porezag, T. Frauenheim, T. Köhler, G. Seifert, and R. Kaschner, Phys. Rev. B **51**, 12947 (1995).

[18] G. Seifert, D. Porezag, and T. Frauenheim, Int. J. Quantum Chemistry **58**, 185 (1996).

[19] M. Elstner, D. Porezag, G. Jungnickel, J. Elsner, M. Haugk, T. Frauenheim, S. Suhai, and G. Seifert, Phys. Rev. B **58**, 7260 (1998).

[20] C. Köhler, G. Seifert, and T. Frauenheim, Chem. Phys. **309**, 23 (2005).

[21] G. Seifert, J. Phys. Chem. A **111**, 5609 (2007).

[22] B. Aradi, B. Hourahine, and Th. Frauenheim, J. Phys. Chem. A, **111**, 5678 (2007).

[23] J. Harris, Phys. Rev. B **31**, 1770, 1985.

[24] W. Foulkes and R. Haydock, Phys. Rev. B **39**, 12520 (1989).

[25] W. M. C. Foulkes and R. Haydock, Phys. Rev. B **39**, 12520 (1989).

[26] E. J. McEniry, R. Drautz and G. K. H. Madsen, J. Phys.: Condens. Matter 25, 115502 (2013).

[27] N. Goldman, S. G. Srinivasan, S. Hamel, L. E. Fried, M. Gaus, and M. Elstner, J. Phys. Chem. C **117**, 7885 (2013).

[28] G. Kresse, Vienna ab initio simulation package, Technische Universitat Wien 1999 Hafner, J. Phys. Rev. B **47**, 558 (1993).

[29] G. Kresse and Furthmuller, J. Phys. Rev. B **54**, 11169 (1996).

[30] G. Kern, J. Hafner and G. Kresse, Surf. Sci. **336**, 464 (1996).

[31] A. A. Stekolnikov, J. Furthmüller, and F. Bechstedt, Phys. Rev. B **65**, 115318 (2002).

[32] J. Hutter and H. P. Luthi, J. Chem. Phys. **101**, 2213 (1994).

[33] K. Raghavachari, D. L. Strout, G. K. Odom, G. E. Scuseria, J. A. Pople, B. G. Johnson, and P. M. W. Gill, Chem. Phys. Lett. **214**, 357 (1993).

[34] B. L. Zhang, C. Z. Wang, K. M. Ho, C. H. Xu, and C. T. Chan, J. Chem. Phys. **97**, 5007 (1992).

[35] R. O. Jones and G. Seifert, Phys. Rev. Lett. **79**, 443 (1997).

[36] W. C. Lu, C. Z. Wang, L. Z. Zhao, W. Zhang, W. Qin, and K. M. Ho, PCCP **12**, 8551 (2010).

[37] L. Z. Zhao, W. S. Su, W. C. Lu, C. Z. Wang, and K. M. Ho, J. Compt. Chem. **32**, 1271 (2011).

[38] M. J. Frisch, G.. W. Trucks, H. B. Schlegel, G. E. Scuseria, M. A. Robb, et al., GAUSSIAN03, Revision D.01, Gaussian, Wallingford CT, 2004.

[39] R. J. VanZee, R. F. Ferrante, K. J. Zeringue, and W. Weltner, Jr., J. Chern. Phys. **86**, 5112 (1987); **88**, 3465 (1988).

[40] J. Hwang, A. YanOrden, K. Tanaka, E. W. Kuo, J. R. Heath, and R. J. Saykally, Mol. Phys. **79**, 769 (1993).

[41] A. Harada, F. Shimojo, and K. Hoshino, Journal of Non-Crystalline Solids **353**, 3519 (2007).

[42] G. Kresse, Journal of Non-Crystalline Solids **312-314**, 52 (2002).

[43] I. Štich, R. Car and M. Parrinello, Phys. Rev. Lett. **63**, 2240 (1989).

TABLE I. Hamiltonian matrices for equilateral triangle Si_3 (Si–Si = 2.35 Å): H^{PBE} is obtained from a deformed minimal basis set of QUAMBOs at PBE/6-31G(d), $H^{fit\text{-}Si3}$ is resulted from the 3c-TB model fitted for only Si_3, and $H^{3c\text{-}TB}$ corresponds to the 3c-TB potential model of Si.[a]

	s_1	px_1	py_1	pz_1	s_2	px_2	py_2	pz_2
H^{PBE}								
s_1	-11.65	0.00	-1.73	-1.02	-4.80	0.00	6.08	-0.51
px_1	0.00	-4.48	0.00	0.00	0.00	-2.45	0.00	0.00
py_1	-1.73	0.00	-6.52	-0.81	-6.08	0.00	4.02	-0.74
pz_1	-1.02	0.00	-0.81	-5.76	-0.51	0.00	0.74	-3.00
$H^{fit\text{-}Si3}$								
s_1	-12.22	0.00	-1.04	-0.60	-4.82	0.00	6.11	-0.48
px_1	0.00	-4.61	0.00	0.00	0.00	-2.46	0.00	0.00
py_1	-1.04	0.00	-6.34	-0.60	-6.11	0.00	4.09	-0.75
pz_1	-0.60	0.00	-0.60	-5.65	-0.48	0.00	0.75	-2.99
$H^{3c\text{-}TB}$								
s_1	-12.72	0.00	-1.07	-0.62	-5.21	0.00	4.50	-0.18
px_1	0.00	-4.59	0.00	0.00	0.00	-2.10	0.00	0.00
py_1	-1.07	0.00	-5.55	-0.33	-4.50	0.00	3.53	-0.22
pz_1	-0.62	0.00	-0.33	-5.17	-0.18	0.00	0.22	-2.10

[a]If we only fit the Si_3 matrix elements by the 3c-TB potential model, the fitted matrix elements can be close to the DFT-PBE H_{Si3} matrix elements. When we need to give considerations to all of the matrix elements, energies and bands of various bulk and cluster structures, the fitted matrix elements would be relaxed.

TABLE II. 3c-TB parameters of C and Si for the repulsive energy functions, free orbital energies (ε^0_s and ε^0_p), overlap (s), and hoppings (h, h^B and h^C) with respect to the two and 3-center interaction and crystal field terms.

	C				**Si**			
Repulsive energy[a]								
	a_1	a_2	a_3	A_4	a_1	a_2	a_3	a_4
χ	248.4353	-2.4382	2.1280	1.0000	344.7310	-3.5743	0.8720	1.0000
χ^{3c}	0.0000	0.0000	0.0000	0.0000	107.4441	-0.0436	0.1728	5.6406
Atomic s and p orbital energies								
	ε^0_s	-14.36	ε^0_p	-5.16	ε^0_s	-11.60	ε^0_p	-4.15
Overlap[a]								
	s_{ss}	s_{sp}	$s_{pp\sigma}$	$s_{pp\pi}$	s_{ss}	s_{sp}	$s_{pp\sigma}$	$s_{pp\pi}$
a_1	-1.4650	0.4066	0.2461	-0.5440	-1.2986	0.5124	0.2746	-1.5103
a_2	0.0000	0.0000	0.0000	0.0000	0.0000	0.0000	0.0000	0.0000
a_3	1.4823	1.1644	1.2069	1.2188	0.9009	0.9899	0.8758	1.1522
a_4	0.0000	0.6160	1.4659	0.0000	0.0000	1.2779	2.3961	0.0000
Hoppings for two-center Hamiltonian[a]								
	h_{ss}	h_{sp}	$h_{pp\sigma}$	$h_{pp\pi}$	h_{ss}	h_{sp}	$h_{pp\sigma}$	$h_{pp\pi}$
a_1	39.3258	-12.8401	-6.4760	25.8463	27.4672	-8.9278	-3.6520	32.6560
a_2	0.0000	0.0000	0.0000	0.0000	-0.1095	-0.1523	-0.0823	-0.1415
a_3	1.5211	1.4728	1.5035	1.9668	0.9634	1.0553	1.0295	1.4298
a_4	0.0000	0.6139	1.1250	0.0000	0.0000	1.2760	2.2814	0.0000
B matrix of the 3-center interaction[a]								
	h^B_{ss}	h^B_{sp}	$h^B_{pp\sigma}$	$h^B_{pp\pi}$	h^B_{ss}	h^B_{sp}	$h^B_{pp\sigma}$	$h^B_{pp\pi}$
a_1	2.3231	-1.1704	-0.9020	4.8561	2.2000	-1.0444	-0.4220	5.6975
a_2, a_3 and a_4 are same as those of h_{ss}, h_{sp}, $h_{pp\sigma}$, and $h_{pp\pi}$.								
C matrix of the crystal field[a]								
	h^C_{ss}	h^C_{sp}	$h^C_{pp\sigma}$	$h^C_{pp\pi}$	h^C_{ss}	h^C_{sp}	$h^C_{pp\sigma}$	$h^C_{pp\pi}$
a_1	2.6722	-1.3463	-1.0376	5.5858	1.8067	-1.4218	-0.7898	7.7626
a_2, a_3 and a_4 are same as those of h_{ss}, h_{sp}, $h_{pp\sigma}$, and $h_{pp\pi}$.								
Interaction range[b]								
r_{max} = 4.8 Å					r_{max} = 6.5 Å			
r_{match} = 4.4 Å					r_{match} = 6.4 Å			
r_{min} = 0.7 × a_4 ($s_{pp\sigma}$) = 1.0 Å					r_{min} = 0.8 × a_4 ($s_{pp\sigma}$) = 1.9 Å			

[a] $\mu = a_1 r^{a_2}[(1-e^{-a_3(r-a_4)})^2 - 1]$ ($\mu = h, h^B, h^C$ and s); χ (or χ^{3c}) $= a_1 r^{a_2} e^{-a_3 r^{a_4}}$.

[b] r_{max} is the cutoff distance for the interaction. r_{match} is a starting point at which an attenuation function is added, i.e., for $r_{match} < r < r_{max}$, $\mu = \mu \times \cos^2[0.5\pi \times (r - r_{match})/(r_{max} - r_{match})]$ ($\mu = h, h^B, h^C, s, \chi$ and χ^{3c}). For $r < r_{min}$, set $\mu(r) = \mu(r_{min})$ ($\mu = h, h^B, h^C$ and s), while χ and χ^{3c} are not submitted to this setup.

Figure captions

FIG. 1. (Color online) Illustration of the 3c-TB Hamiltonian model. $H^{2c}_{1s,,2pz}= 0$, $H^{2c}_{1py,2pz}= 0$ in the two-center approximation; but the 3-center corrections $H^{3c}_{1s,,2pz} \neq 0$, $H^{3c}_{1py,2pz} \neq 0$; and the crystal field effect H^{cf} leads to lower *s* and *p* orbital energies and a splitting of p_x, p_y, and p_z energy levels.

FIG. 2. (Color online) 3c-TB energy bands (dotted line) of C in the diamond, graphene, SC, and BCC structures compared with the DFT-PW91 (solid line) and DFTB (circle line) calculated results.

FIG. 3. (Color online) 3c-TB energy bands (dotted line) of Si in the diamond, SC, BCC, and FCC structures compared with the DFT-PW91 (solid line) and DFTB (circle line) calculated results.

FIG. 4. (Color online) Binding energies per atom (E_b) from the 3c-TB and DFTB calculations for C and Si compared with the DFT-PW91 calculated results. The DFT-PW91 energies were shifted in order to make the binding energies of the C and Si diamond structures consistent with the experimental data of -7.37 and -4.67 eV, respectively. For comparison, the DFTB energies were also shifted to make the binding energies of diamond structures at equilibrium bond lengths equal to the DFT-PW91 values.

FIG. 5. (Color online) Binding energies per atom (E_b) relative to free singlet C or Si atoms of the C_n and Si_n clusters calculated at 3c-TB, compared with the calculated results at DFTB, and DFT-B3LYP/6-31G(d) for C and DFT-PBEPBE/6-31G(d) for Si. The absolute binding energies at DFT are much lower than the TB data, since in the data fitting of the TB parameters, the DFT energies were shifted upwards to make the binding energy of the C and Si diamond structures consistent with the experimental values -7.37 eV (C) and -4.67 eV (Si).

FIG. 6. (Color online) Scatter plot of the binding energies per atom from the TB/DFTB calculations verses those from the calculations at DFT-B3LYP for C_n and DFT-PBEPBE for Si_n with n denoted in Fig. 5.

FIG. 7. (Color online) 3c-TB optimized structures of $C_{8,14,20,32}$ and $Si_{7,10,20,32}$, compared with the DFT-B3LYP/6-31G(d) optimized C_n and DFT-PBEPBE/6-31G(d) optimized Si_n cluster structures. The atoms in light color for Si_{32} denote the embedded atoms.

FIG. 8. (Color online) Pair correlation function *g(r)* for (a) liquid carbon and (b) liquid silicon obtained from the TBMD simulations using the 3c-TB potential model are compared with the first-principles simulated results (Refs. 41 and 42).

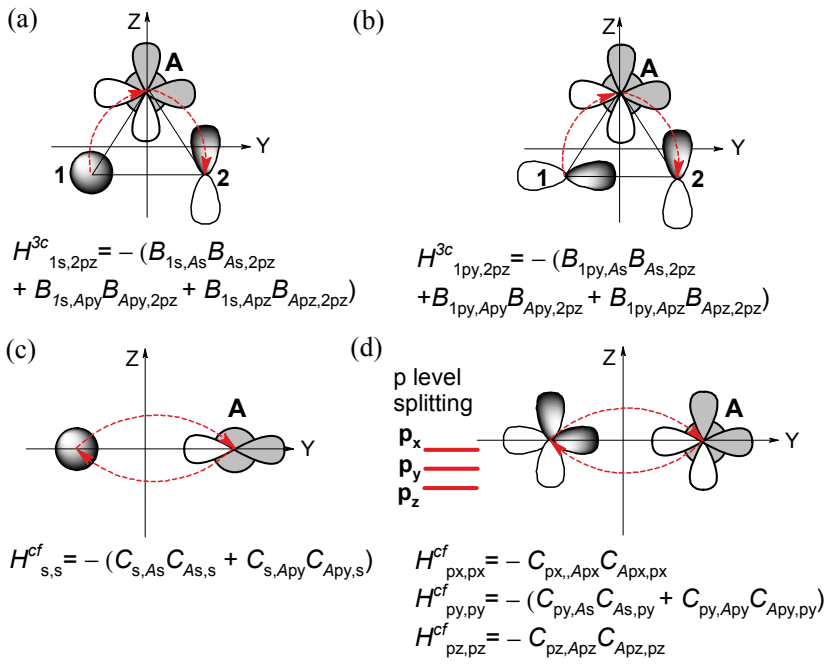

FIG. 1. (Color online) Illustration of the 3c-TB Hamiltonian model. $H^{2c}_{1s,,2pz} = 0$, $H^{2c}_{1py,2pz} = 0$ in the two-center approximation; but the 3-center corrections $H^{3c}_{1s,,2pz} \neq 0$, $H^{3c}_{1py,2pz} \neq 0$; and the crystal field effect H^{cf} leads to lower *s* and *p* orbital energies and a splitting of p_x, p_y, and p_z energy levels.

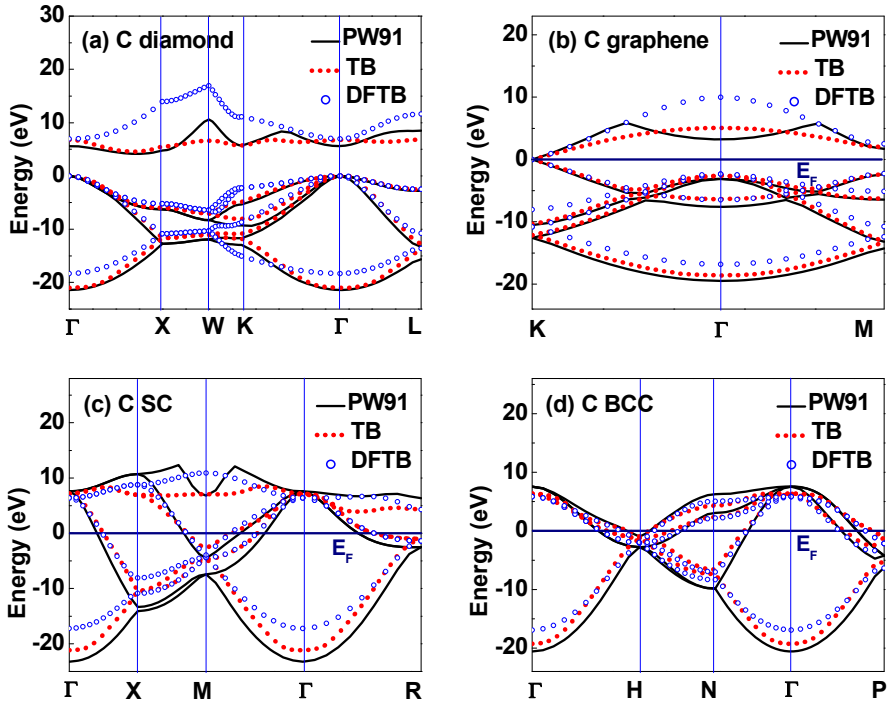

FIG. 2. (Color online) 3c-TB energy bands (dotted line) of C in the diamond, graphene, SC, and BCC structures compared with the DFT-PW91 (solid line) and DFTB (circle line) calculated results.

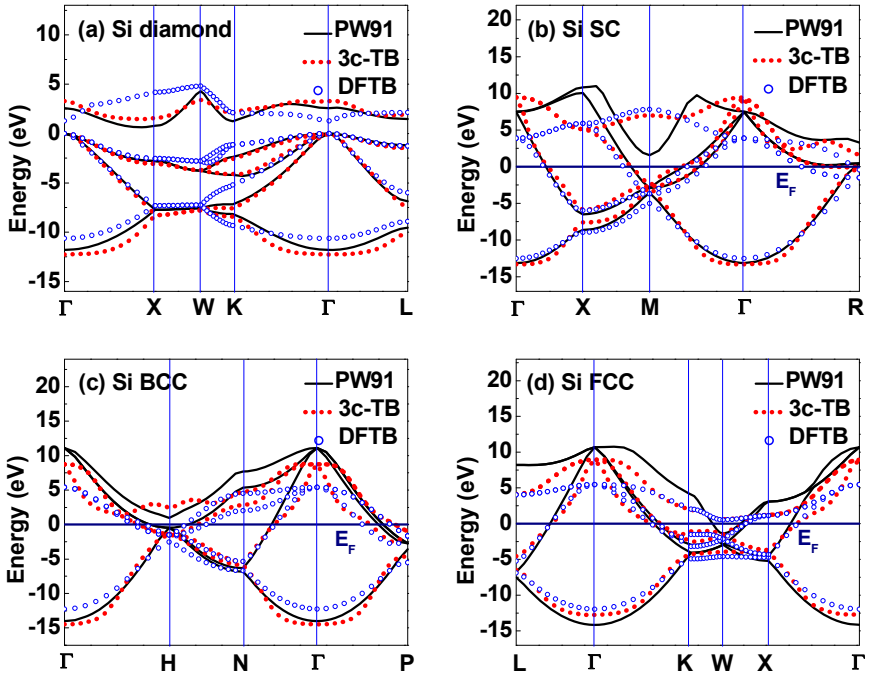

FIG. 3. (Color online) 3c-TB energy bands (dotted line) of Si in the diamond, SC, BCC, and FCC structures compared with the DFT-PW91 (solid line) and DFTB (circle line) calculated results.

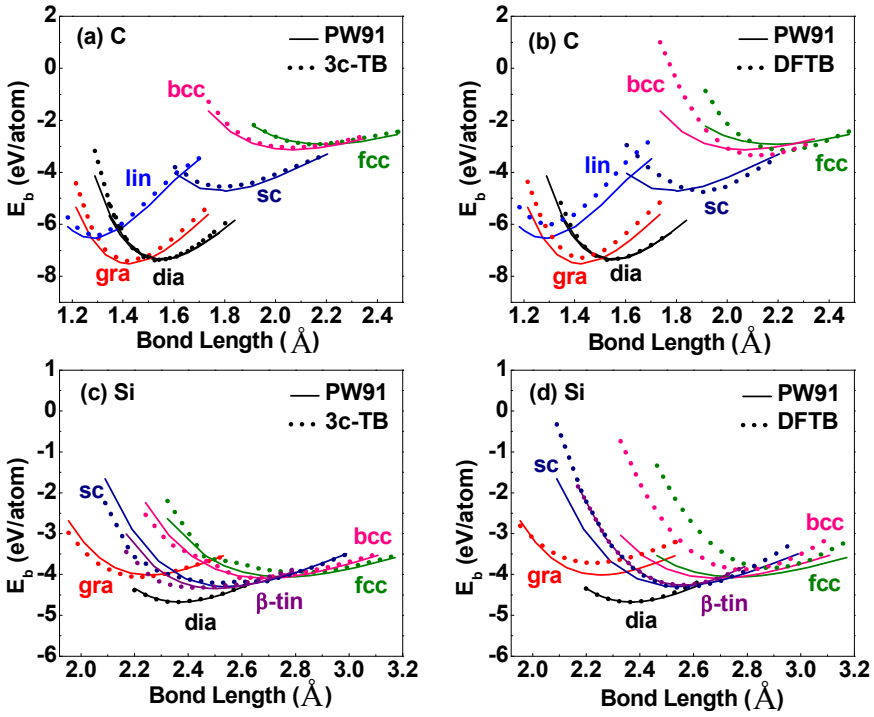

FIG. 4. (Color online) Binding energies per atom (E_b) from the 3c-TB and DFTB calculations for C and Si compared with the DFT-PW91 calculated results. The DFT-PW91 energies were shifted in order to make the binding energies of the C and Si diamond structures consistent with the experimental data of -7.37 and -4.67 eV, respectively. For comparison, the DFTB energies were also shifted to make the binding energies of diamond structures at equilibrium bond lengths equal to the DFT-PW91 values.

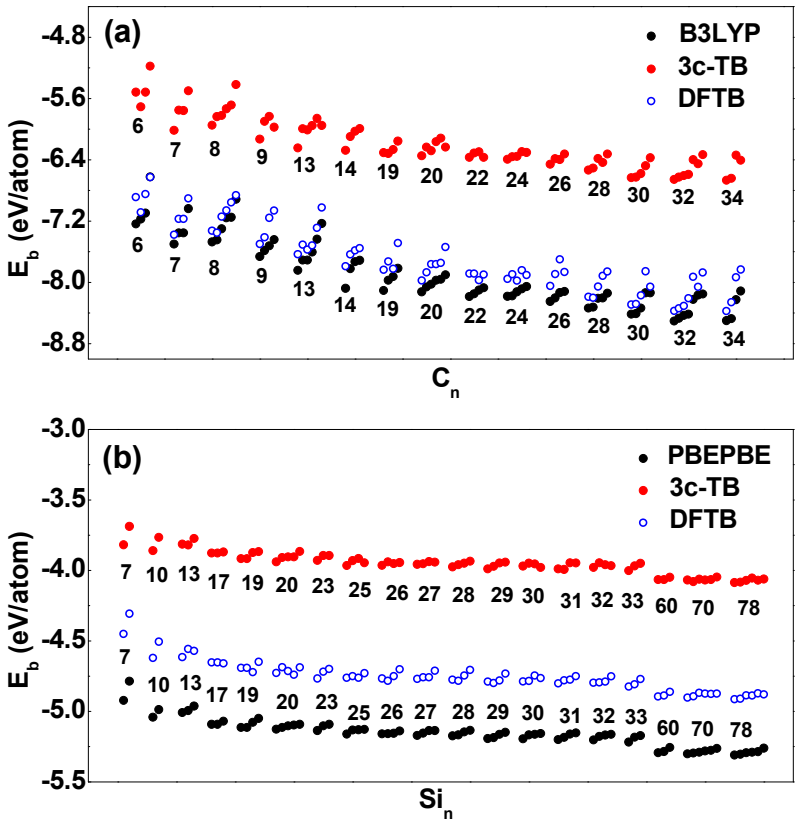

FIG. 5. (Color online) Binding energies per atom (E_b) relative to free singlet C or Si atoms of the C_n and Si_n clusters calculated at 3c-TB, compared with the calculated results at DFTB, and DFT-B3LYP/6-31G(d) for C and DFT-PBEPBE/6-31G(d) for Si. The absolute binding energies at DFT are much lower than the TB data, since in the data fitting of the TB parameters, the DFT energies were shifted upwards to make the binding energy of the C and Si diamond structures consistent with the experimental values -7.37 eV (C) and -4.67 eV (Si).

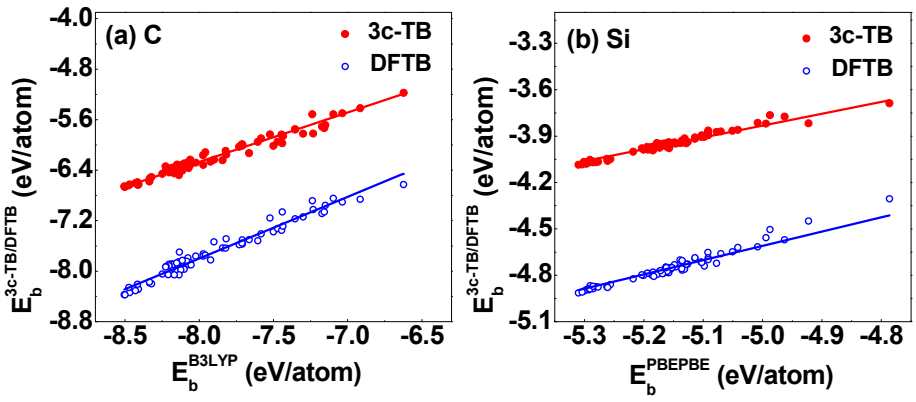

FIG. 6. (Color online) Scatter plot of the binding energies per atom from the TB/DFTB calculations verses those from the calculations at DFT-B3LYP for C_n and DFT-PBEPBE for Si_n with n denoted in Fig. 5.

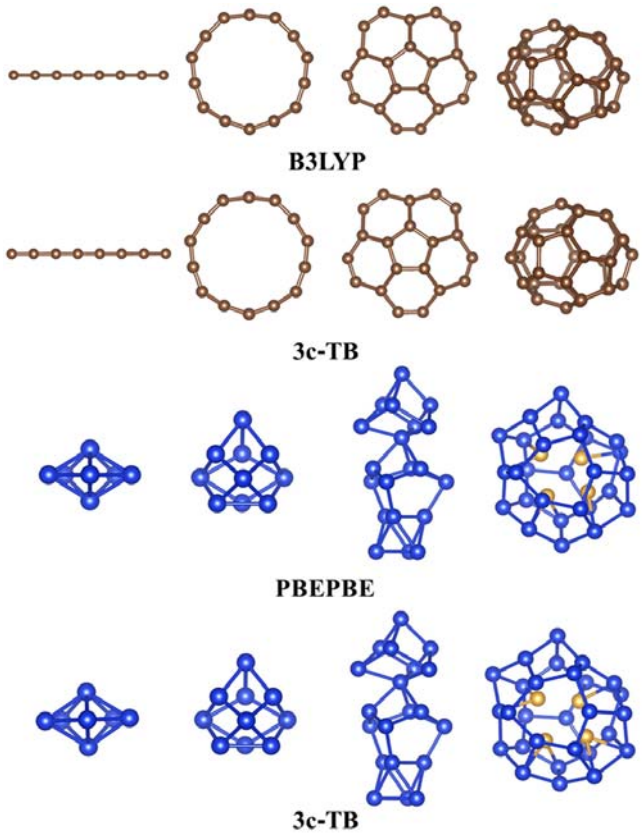

FIG. 7. (Color online) 3c-TB optimized structures of $C_{8,14,20,32}$ and $Si_{7,10,20,32}$, compared with the DFT-B3LYP/6-31G(d) optimized C_n and DFT-PBEPBE/6-31G(d) optimized Si_n cluster structures. The atoms in light color for Si_{32} denote the embedded atoms.

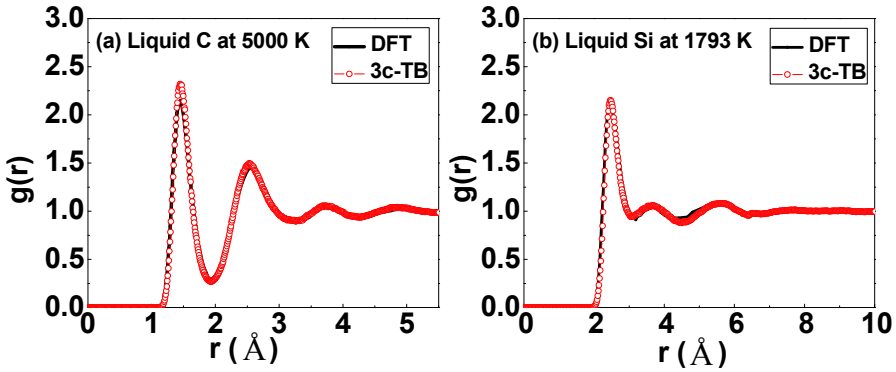

FIG. 8. (Color online) Pair correlation function *g(r)* for (a) liquid carbon and (b) liquid silicon obtained from the TBMD simulations using the 3c-TB potential model are compared with the first-principles simulated results (Refs. 41 and 42).